# Detailed analysis of scanning tunneling microscopy images of the Si(001) reconstructed surface with buckled dimers

Hiromi Okada, Yoshitaka Fujimoto, Katsuyoshi Endo, Kikuji Hirose, and Yuzo Mori
*Department of Precision Science and Technology, Osaka University, Suita, Osaka 565-0871, Japan*
(Received 15 June 2000; revised manuscript received 22 January 2001; published 1 May 2001)

An adequate interpretation of scanning tunneling microscopy (STM) images of the clean Si(001) surface is presented. We have performed both STM observations and *ab initio* simulations of STM images for buckled dimers at the $S_A$ step of the clean Si(001) surface. By comparing experimental results with theoretical ones, it is revealed that STM images depend on the sample bias and the tip-sample separation. This enables us to elucidate the relationship between the corrugation in STM images and the atomic structure of buckled dimers. Moreover, to elucidate these changes, we analyze details of the spatial distributions of the $\pi,\pi^*$ surface states and $\sigma,\sigma^*$ Si-Si bond states in the local density of states, which contribute to STM images.

DOI: 10.1103/PhysRevB.63.195324 PACS number(s): 68.37.Ef

## I. INTRODUCTION

Scanning tunneling microscopy (STM) has provided much useful information on surface configurations, with atomic resolution. The clean Si(001) surface has been much studied by STM because of the great fundamental and technological importance of semiconductor devices. In STM images of the $2\times1$ structure on terraces, silicon dimers appear to be symmetric at room temperature due to the time averaging of the flipflop motion of the buckled dimers, while at temperatures below $\sim200$ K the stable configuration is the $c(4\times2)$ or $p(2\times2)$ structure consisting of asymmetric dimer rows.[1–3] For the $c(4\times2)$ structure, the dependence of the STM image on the bias voltage at 80 K has been studied in detail.[4] On the other hand, the behavior of the dimers at step edges differs from that on the terraces. For example, the dimers at $S_A$ steps are observed to be buckled at both low and room temperatures.[5] However, a detailed observation of the $S_A$ steps has not been exhaustively carried out, since filled- and empty-state images at only a few bias voltages have been reported.[6]

It is known that STM images reflect electronic structure rather than atomic geometry. Consequently, bias-dependent STM images result from variations of the spatial distribution of the local density of states (LDOS) which is a function of energy. Therefore, to interpret STM images properly, the spatial distributions of the LDOS must be calculated strictly by *ab initio* methods. Some authors have attempted to compare experimental STM images with theoretical ones for the Si(001) reconstructed surface.[4,7] Kageshima and Tsukada carried out a simulation of polarity-dependent STM images of Si(001). However, their investigation was based on a semiempirical method with linearly combined atomic orbitals.[7] Hata *et al.* pointed out that the $\pi,\pi^*$ surface states and $\sigma,\sigma^*$ bulk ones contribute to the STM images, by calculating the spatial distributions of those states localized near the outermost atoms.[4] These results emphasize that a reproduction of the STM image from the calculated spatial distribution of the LDOS is very important. But such research is still limited at present.

In this paper, we present an improved interpretation of STM images and provide a more profound understanding of the electronic structure for the clean Si(001) surface. STM observations are performed on the buckled dimers at the $S_A$ step of the clean Si(001) surface. They are strongly dependent on the applied bias voltage and the tip-sample separation, which is confirmed by *ab initio* simulations. The STM images are interpreted as isosurfaces of the spatial distribution of the LDOS in the vacuum region between a tip and a sample, which is very different from the behavior of the LDOS near the outermost atoms. Moreover, the calculated LDOS shows how the spatial distributions of the characteristic surface ($\pi$, $\pi_1^*$, and $\pi_2^*$ dangling-bond states) and bulk states ($\sigma$ and $\sigma^*$ Si-Si bond states) contribute to the bias dependence of the STM images.

## II. METHODS OF STM OBSERVATION AND THEORETICAL CALCULATION

### A. STM observations

Experiments were performed in an ultrahigh-vacuum (UHV) chamber equipped with a STM. The base pressure was less than $1\times10^{-8}$ Pa. The samples were Si(001) (B doped, 0.2–0.5 $\Omega$cm) wafers. They were degassed at 900 K overnight, flashed to 1450 K for 30 sec, and then cooled to room temperature to prepare the clean Si(001)-$2\times1$ surface. The tips were prepared by the electrochemical etching of a polycrystalline tungsten wire and cleaned by electron bombardment in UHV prior to use. Constant-current STM images were obtained at room temperature.

### B. Theoretical calculations

The *ab initio* electronic states calculations were performed by the self-consistent pseudopotential method within density-functional theory.[8] The exchange-correlation interaction was treated by the Ceperley-Alder form in the local-density approximation (LDA).[9] Norm-conserving Troullier-Martins pseudopotentials[10] were used in a separable nonlocal form.[11] The wave functions were expanded in a plane-wave basis set with a cutoff energy of 16 Ry.

Figure 1 shows the structure of the clean Si(001) surface with the $S_A$ step. This structure was simulated by a repeated

 

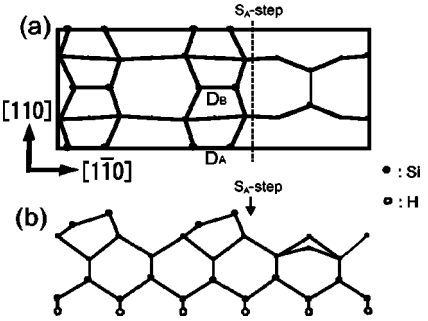


FIG. 1. The simulation model of the Si(001) surface with an $S_A$ step: (a) top view; (b) side view.

slab geometry. The unit supercell for the stepped Si(001) surface contained five silicon layers, the lowest of which was terminated by hydrogen atoms, and the width of the vacuum region was equivalent to that of 12 silicon layers. The four outermost silicon layers were fully optimized by the *ab initio* molecular-dynamics method.[12]

Many theoretical STM images have been generated in the Tersoff-Hamann approximation.[13–15] This method is actually valid for many systems despite its extreme simplicity.[16–24] In this scheme, the tunneling current is proportional to the surface LDOS at the tip position integrated over an energy range restricted by the applied bias voltage. We calculated the LDOS $\rho_s(x,y,z;\epsilon)$ at spatial points $(x,y,z)$ and energy $\epsilon$ by sampling 100 $k$ points of the surface Brillouin zone (SBZ). The STM images were generated from the isosurface of the spatial distribution formed by integration of the LDOS over the energy range from the Fermi energy $E_F$ to $E_F - eV$ with applied voltage $V$, i.e., $\int_0^{eV}\rho_s(x,y,z;E_F-eV+\epsilon)d\epsilon$. Hereafter, we refer to this ''energy-integrated LDOS'' as the EI-LDOS. Thereby the computed STM images correspond to experimental constant-current images.

## III. RESULTS AND DISCUSSION

### A. Optimized atomic structure and electronic structure of the stepped Si(001) surface

The atomic structure of the stepped Si(001) surface was optimized by minimizing the total energy. Both of the calculated bond lengths of $D_A$ and $D_B$ dimers indicated in Fig. 1 were 2.36 Å. This value is similar to the dimer bond length of 2.38 Å for the $p(2\times2)$ reconstruction reported by Shkrebtii *et al.*,[25] and is longer than the 2.28 Å found by Ramstad *et al.*[26] and 2.31 Å by Gunnella *et al.*[27] for the Si(001)-$p(2\times2)$ surface. We obtained the backbond lengths of the upper and lower atoms to be 2.38 and 2.33 Å, respectively, which are longer than the values of 2.34 and 2.31 Å reported by Ramstad *et al.*[26] and 2.33 and 2.30 Å by Gunnella *et al.*[27]

We calculated the band structure for the optimized Si(001) surface with an $S_A$ step. This is formed at 100 equidistant points along the Bloch wave vector $\mathbf{k}_\parallel$ in the two-dimensional (001) SBZ. Figure 2 shows the band structure for the stepped Si(001) surface along high-symmetry directions of the SBZ. The single-particle calculation within the LDA is well known to underestimate the band gap. Although

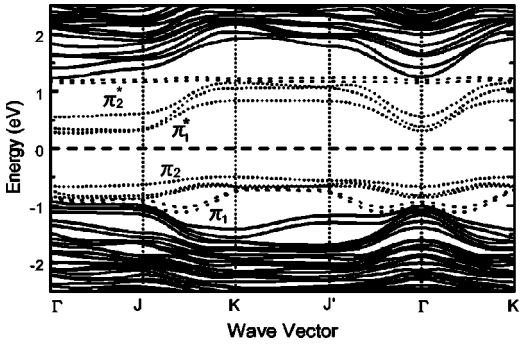


FIG. 2. Band structure of the stepped Si(001) surface optimized by molecular dynamics. Eigenvalues in the empty states are rigidly shifted by 0.63 eV. To match our STM results, the Fermi energy $E_F$ position is determined at 0.6 eV above the valence-band top.

the band gap is calculated as 0.13 eV, all empty states of the band structure must shift rigidly upward in energy by 0.63 eV.[28–30] This value was determined from the results of angle-resolved photoemission,[31] angle-resolved inverse photoemission,[32] and scanning tunneling spectroscopy (STS).[33] The position of the Fermi energy ($E_F$) is determined at about 0.6 eV above the valence-band top and about 0.2 eV below the conduction-band bottom in order to coincide with our STM results.

As shown in Fig. 2, filled $\pi$ (empty $\pi^*$) surface states separate into bunches of filled $\pi_1$ and $\pi_2$ (empty $\pi_1^*$ and $\pi_2^*$) surface states in the bulk band gap. These bunchings arise from the existence of the step, since each of the $\pi_1$, $\pi_2$, $\pi_1^*$ and $\pi_2^*$ surface states is represented by one curve in the case of the Si(001)-$p(2\times2)$ surface.[26,34,35] The filled $\pi_1$ and $\pi_2$ states disperse from $-1.3$ to $-0.6$ eV. Although the empty $\pi_1^*$ state spreads widely from $+0.2$ to $+1.1$ eV, the empty $\pi_2^*$ state spreads at around $+1.1$ eV. These features are similar to the results of calculations for the $p(2\times2)$ surface.[26,34,35]

### B. Comparison of experimental STM images with simulated ones

We aimed at obtaining STM images of a buckled dimer row at an $S_A$ step on the clean Si(001)-$2\times1$ surface under different sample-bias conditions. Figures 3 (filled states) and 4 (empty states) show the experimental STM images of the $S_A$ step and the simulated ones of stepped Si(001). All STM images in Figs. 3 and 4 were obtained at a tunneling current of 0.5 nA, and simulated images were generated by the EI-LDOS of $1.5\times10^{-4}$ electrons/Å$^3$. The simulated images accurately reproduce the experimental results.

In the experimental images of filled states [Figs. 3(a) and 3(c)], the dimer row at the $S_A$ step makes a zigzag pattern. In other words, one atom in a buckled dimer is bright and the other is absent.[1–6] The filled-state images do not change greatly in the range of bias voltage from $-1.0$ to $-2.5$ V, except for the difference in the corrugation height. The simulated filled-state images [Figs. 3(b) and 3(d)] imply that the bright protrusion of the buckled dimer in the experimental images corresponds to the upper atom of the buckled dimer.

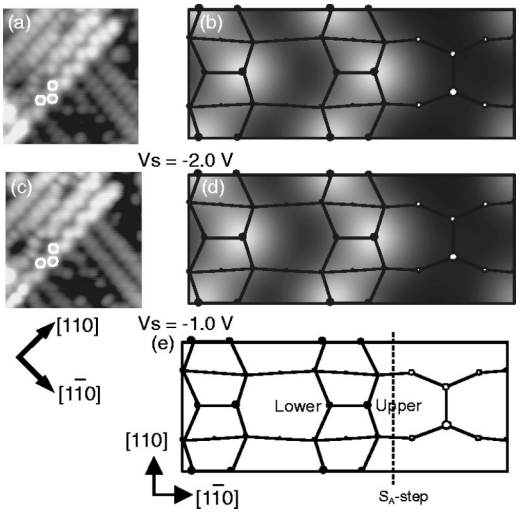


FIG. 3. Filled-state STM images ($5\times5$ nm$^2$) of the $S_A$ step on the Si(001)-$2\times1$ surface at room temperature (left column) and simulated ones of the Si(001) surface with the $S_A$ step (right column). These experimental images were obtained at sample biases of (a) $-2.0$ and (c) $-1.0$ V and at a tunneling current of 0.5 nA. The simulated images were generated from isosurfaces of the EI-LDOS [(b) 0 to $-2.0$ and (d) 0 to $-1.0$ eV] of $1.5\times10^{-4}$ electrons/Å$^3$. The maximal heights of these isosurfaces are (b) 4.3 and (d) 4.1 Å from the upper atom. The atomic positions in these images are represented in (e) and the smallest filled circles are the second-layer atoms.

On the other hand, the empty-state images of the buckled dimer at the $S_A$ step show dramatic changes at room temperature as the sample bias is increased. These images can be divided into three typical types depending on applied voltage: (i) below $+1.1$ V, (ii) at about $+1.2$ V, and (iii) from $+1.3$ to $+2.0$ V. The empty-state images in Fig. 4 were obtained for the same area as shown in Fig. 3. At a sample bias of $+0.6$ V in Fig. 4(a), the zigzag corrugation reverses from that in the filled-state images in Figs. 3(a) and 3(c).[6] This reversal is also observed on the terrace for the Si(001)-$c(4\times2)$ surface at low temperatures.[3,4] Inside one buckled dimer in Fig. 4, two protrusions are clearly distinguished. One is brighter than the other, which cannot be seen in the filled states [Figs. 3(a) and 3(c)]. The simulated STM image at a sample bias of $+0.6$ eV in Fig. 4(b) coincides with the experimental one [Fig. 4(a)]. The brighter protrusion in Fig. 4(a) corresponds to the lower atom of the buckled dimer. When $+1.2$ V is applied to the sample, the experimental and simulated images show that the zigzag dimer row changes into a symmetric one [Figs. 4(c) and 4(d)]. At a sample bias of $+1.5$ V in Fig. 4(e), the brighter oval-shaped protrusion is located at the opposite side from that at a sample bias of $+0.6$ V in the buckled dimer. The atomic protrusions align parallel to the dimer rows. In addition, a deep trough appears in the middle of the dimer row, as indicated by black arrows in Fig. 4(e). This has been observed in the empty-state images at high biases at both room and low temperatures.[4,36–38] These features are accurately represented in the simulated image, as shown in Fig. 4(f). The bright protrusion corresponds to the upper atom of the buckled dimer.

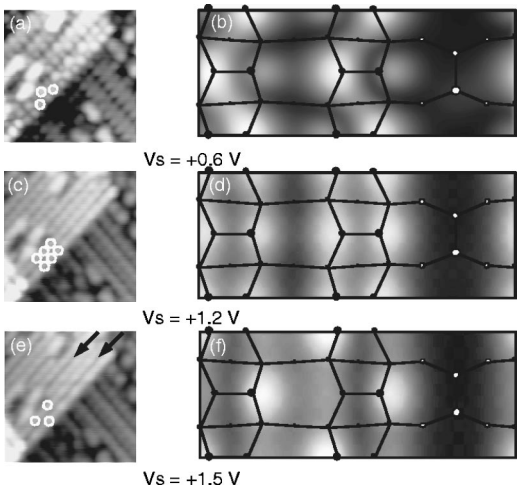


FIG. 4. Empty-state STM images ($5\times5$ nm$^2$) of the $S_A$ step on the Si(001)-$2\times1$ surface at room temperature (left column) and simulated ones of the Si(001) surface with the $S_A$ step (right column). These experimental images are obtained at sample biases of (a) $+0.6$, (c) $+1.2$, and (e) $+1.5$ V and at a tunneling current of 0.5 nA. The simulated images were generated at isosurfaces of the EI-LDOS [(b) 0 to $+0.6$, (d) 0 to $+1.2$, and (f) 0 to $+1.5$ eV] of $1.5\times10^{-4}$ electrons/Å$^3$. The maximal heights of these isosurfaces are (b) 2.9, (d) 3.5, and (f) 4.3 Å from the upper atom. The atomic positions in these images are represented in Fig. 3(e).

We also investigated the current dependence of buckled dimers and dimer rows on the Si(001) surface in STM images. Figure 5(a) shows STM images of the Si(001)-$2\times1$ surface at a sample bias of 1.5 V. In the upper (lower) area of the image, the tunneling current was 0.5 (5.0) nA. In the upper half of the figure, a deep trough appears in the center of the dimer row, as mentioned above. The deep trough exists in the center of the dimer row indicated by black arrows in Fig. 5(a) (at a tunneling current of 0.5 nA), as mentioned above. When the tunneling current is changed to 5.0 nA, another trough appears between the dimer rows, as indicated by white arrows in Fig. 5(a). Furthermore, the two atoms in

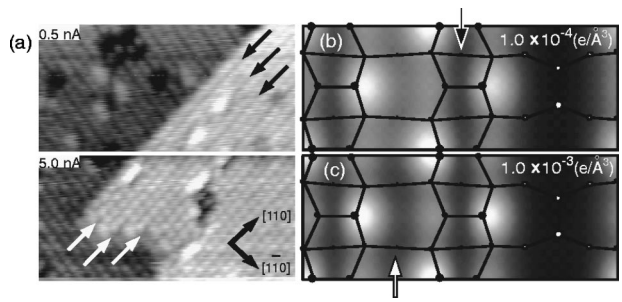


FIG. 5. Current-dependent STM images ($9\times9$ nm$^2$) of the Si(001)-$2\times1$ surface of the empty states at room temperature and the simulated image. (a) The experimental image is obtained at a sample bias of $+1.5$ V. In the upper and lower parts of the STM image, the tunneling current is 0.5 and 5.0 nA, respectively. (b) This image is equivalent to Fig. 4(f). (c) The simulated image is generated by the isosurface of $1.5\times10^{-3}$ electrons/Å$^3$, which is one order of magnitude larger than that adopted in Fig. 4(f). The maximal height of this isosurface is 3.5 Å from the upper atom.

a dimer are clearly visible. Since the tip approaches the sample surface on switching the tunneling current from 0.5 to 5.0 nA, the LDOS at the nearer sample surface contributes to the tunneling current. In Fig. 5(c) the simulated image is generated as the isosurface of $1.5\times10^{-3}$ electrons/Å$^3$, which is one order larger of magnitude than that adopted in Fig. 4(f). This simulated image is consistent with the experimental one and indicates that STM images depend on the magnitude of the surface LDOS, i.e., the tunneling conductance.

Consequently, the simulation of STM images can support the interpretation of the experimental STM images, as shown in Figs. 3, 4, and 5. The simulated ones generated from the EI-LDOS of $1.5\times10^{-4}$ electrons/Å$^3$ correspond well with the experimental STM images obtained at a tunneling current of 0.5 nA. We can estimate the distance from the surface at which the spatial distribution of the EI-LDOS contributes to the tunneling current, i.e., the STM image. When the sample bias and the tunneling current are set to $+1.5$ and 0.5 (5.0) nA, the distance of the EI-LDOS from the surface contributing to the STM images is predicted to be 4.3 (3.5) Å. Similarly, when the tunneling current is fixed to be 0.5 nA, the EI-LDOS at about 4.3, 4.1, 2.9, and 3.5 Å from the surface contributes to the STM images at sample biases of $-2.0$, $-1.0$, $+0.6$, and $+1.2$ V, respectively. As the absolute value of the bias voltage is increased or the tunneling current is decreased, the distance from the surface at which the surface LDOS contributes to the tunneling current becomes larger. When tip-sample separations are assumed to be about twice as long as the distances estimated above, they agree with the experimental values.[24] To estimate the tip-sample separation exactly, both the tip and the sample must be taken into account in the calculation.

### C. LDOS and spatial distribution of each state in LDOS of the stepped Si(001) surface

By calculating the LDOS at different sites on the stepped Si(001) surface, we demonstrate how the spatial distributions of the characteristic surface and bulk states in the LDOS contribute to the STM images.

Figure 6 shows the LDOS at different sites on the stepped Si(001) surface. The LDOS's in Fig. 6(b) are generated at seven specific sites (sites $A$–$G$) in Fig. 6(a), which are located at a height of 4.3 Å above the upper dimer atom. In the filled states, we find a sharp peak at $-0.7$ eV and a broad one at $-1.7$ eV marked by $FS_1$ and $FS_2$, respectively, in Fig. 6(b). These peaks appear similar in every spectrum in Fig. 6(b). By comparing these peaks with the band structure (Fig. 2), we see that $FS_1$ and $FS_2$ mainly correspond to occupied [$\pi$ ($\pi_1$ and $\pi_2$)] dangling-bond states and Si-Si bond ($\sigma$) states, respectively. $FS_1$ and $FS_2$ at the upper atom [site $A$ in Fig. 6(a)] are strongest, while they are weakest at the cave and valley bridge sites [sites $D$ and $G$ in Fig. 6(a)].

For the empty states, the LDOS's have a small peak at around $+0.8$ eV ($ES_1$), a sharp one at $+1.2$ eV ($ES_2$), and a broad one at $+1.8$ eV ($ES_3$), as shown in Fig. 6(b). From the band structure, $ES_1$ and $ES_2$ mainly correspond to unoccupied $\pi_1^*$ and $\pi_2^*$ dangling-bond states, respectively. The

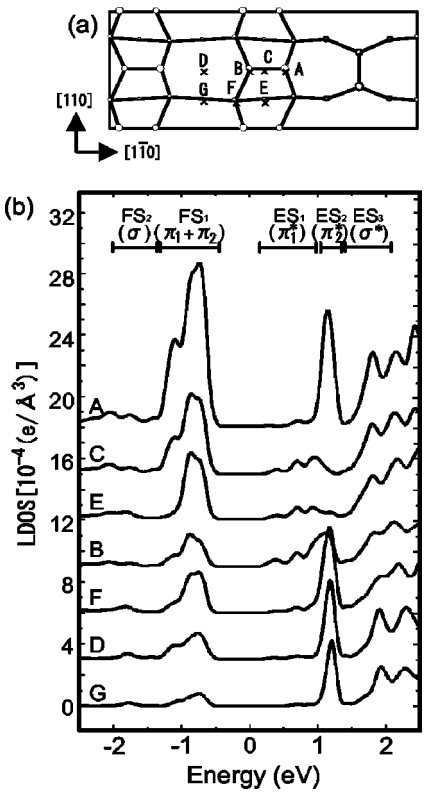


FIG. 6. Calculated LDOS of the stepped Si(001) surface at different sites. (a) Top view indicates the seven sites at which the LDOS's are calculated. *A*, upper atom; *B*, lower atom; *C*, bridge; *D*, cave; *E*, pedestal; *F*, side bridge; and *G*, valley bridge. (b) The LDOS's at these seven sites are generated at the same height of 4.3 Å from the upper atom. The five characteristic peaks at $-0.7$, $-1.7$, $+0.8$, $+1.2$, and $+1.8$ eV are marked $FS_1$, $FS_2$, $ES_1$, $ES_2$, and $ES_3$, respectively.

heights and fine structures of $ES_1$ and $ES_2$ at each site differ greatly from one another, which causes a dramatic change in the empty-state STM images. $ES_1$ at the lower atom, bridge, and pedestal sites [sites $B$, $C$, and $E$ in Fig. 6(a)] are stronger than at other sites. $ES_2$ at the upper atom, cave, side bridge, and valley bridge sites (sites $A$, $D$, $F$, and $G$) are much sharper than at other sites. In contrast, $ES_2$ at the pedestal site (site $E$) decreases markedly. As described below, the analysis of the spatial distribution of each state is useful for understanding STM images.

We compare our calculated LDOS's with previously reported STS measurements for the Si(001)-$2\times1$ surface.[33,36,37] The experimental tunneling spectra $(dI/dV)/(I/V)$ have some characteristic features. (i) The band gap is $\sim0.6$ eV. (ii) In the filled states, a large peak is found around $-0.7$ eV. (iii) In the empty states, two peaks are observed at around $+0.6$ and $+1.3$ eV. These features agree with those of our theoretical LDOS's. We attribute the peaks at $-0.7$, $+0.6$, and $+1.3$ eV to $\pi$, $\pi_1^*$, and $\pi_2^*$, respectively.

We calculate the spatial distribution of each characteristic state by integrating the LDOS's over the energy range in which peaks relating to the state spread are found. Figure 7 shows the spatial distributions of the EI-LDOS's of the two

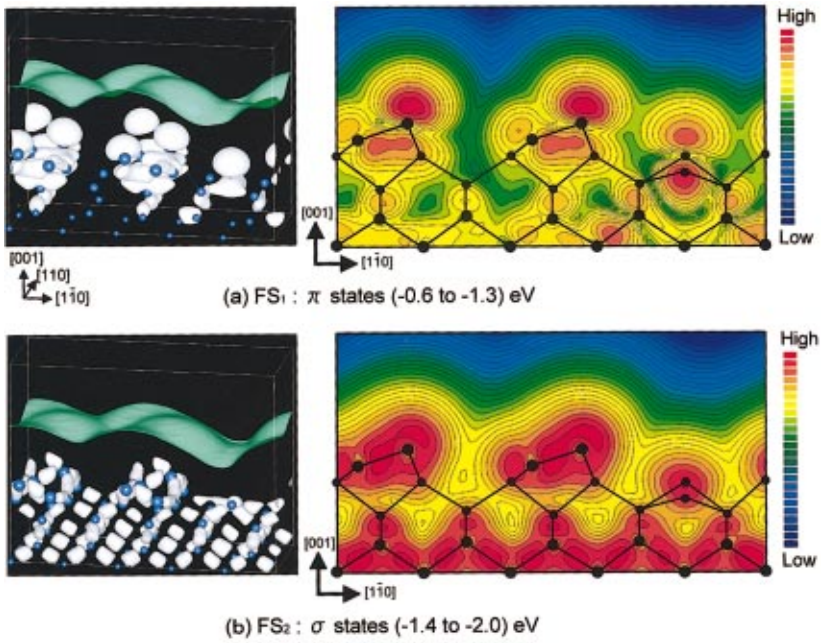


FIG. 7. (Color) Isosurfaces (left panel) and contour plots (right panel) of charge densities for the two characteristic peaks in the filled states: (a) $-0.7$ ($-0.6$ to $-1.3$) and (b) $-1.7$ ($-1.4$ to $-2.0$) eV. Isosurfaces (left panel) in the bulk (white) and the vacuum (at $\sim 4.3$ Å from the upper atom; green) are shown in the same cell; the height of the silicon layers is represented by the size of the ball. Logarithmic contour maps (right panel) are along the cross section in the (110) plane along the $[1\bar{1}0]$ direction including the buckled dimer. The magnitude of the energy-integrated LDOS increases/decreases one order per four contour lines.

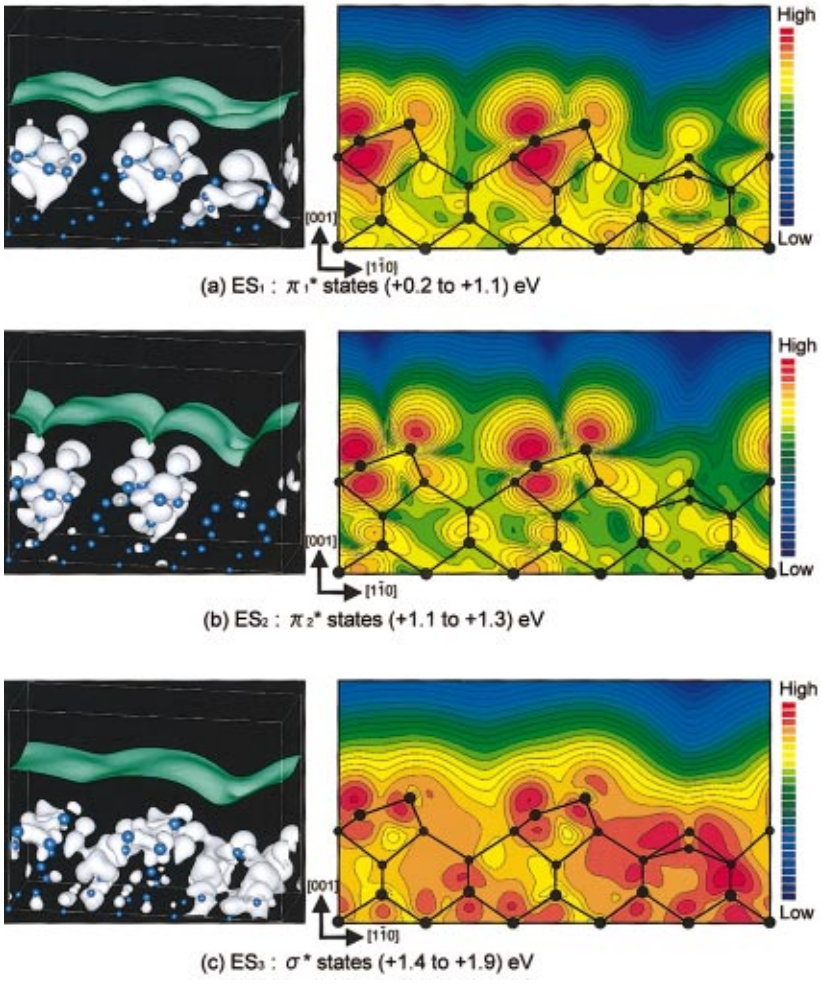


FIG. 8. (Color) Isosurfaces (left panel) and contour plots (right panel) of charge densities for the three characteristic peaks in the empty states: (a) $+0.8$ ($+0.2$–$+1.0$), (b) $+1.2$ ($+1.1$–$+1.3$), and (c) $+1.8$ ($+1.4$–$+2.0$) eV. The meanings of the symbols are the same as in Fig. 7.

characteristic peaks [(a) $FS_1$ and (b) $FS_2$] in the filled states. Figure 7(a) shows that charge transfer occurs from the lower atom to the upper one and the EI-LDOS is largely localized at the upper atom.[39] The maximum EI-LDOS in the vacuum region is located just above the upper atom. For $FS_2$ [Fig. 7(b)], the spatial distribution of the EI-LDOS is largely localized between Si-Si atoms and forms $\sigma$ bonds, which is very different from the $\pi$ surface state ($FS_1$). In contrast, in the vacuum region, the maximum EI-LDOS of $FS_2$ is again located above the upper atom, although the corrugation of contour lines for $FS_2$ is smaller than that for $FS_1$. This feature leads to the similarity of STM images at any sample bias in the filled states, as shown in Fig. 3.

Figure 8 shows the spatial distributions of EI-LDOS's of the three peaks [(a) $ES_1$, (b) $ES_2$, and (c) $ES_3$] in the empty states. In Fig. 8(a), the EI-LDOS of $ES_1$ is localized at the lower atom of the buckled dimer. In the vacuum region, the corrugation of the EI-LDOS has two humps above a buckled dimer and a minimum at the center of the dimer. The hump is considerably larger above the lower atom than above the upper one. $\pi_1^*$ contributes to the STM images at low biases (below $+1.1$ eV). On the other hand, the spatial distribution of $ES_2$ is very different from that of $ES_1$. As shown in Fig. 8(b), a deep minimum appears in the middle of the buckled dimer [sites *C* and *E* in Fig. 6(a)] and the maximum of the EI-LDOS of $ES_2$ extends into the vacuum above the upper atom more than above the lower atom. These striking features of the $\pi_2^*$ state lead to the deep trough in the middle of a dimer row and the bright oval-shaped protrusion at the upper dimer atom in the STM images at sample biases from $+1.2$ to $+2.0$ V, as shown in Figs. 4(e) and 4(f). In addition, we also find that the EI-LDOS of $ES_2$ decays more slowly in vacuum at the cave, valley bridge, and side bridge sites (sites *D*, *F*, and *G*) than at the other sites. This feature explains the changes in the STM image in Fig. 5(a) when the tunneling current is switched from 0.5 to 5.0 nA at a sample bias of $+1.5$ V. In other words, since the tip-sample separation is shorter and the STM image reflects the spatial distribution of the LDOS nearer to the surface, another trough emerges between dimer rows and each atom appears to be clearly resolved. $ES_3$ corresponds to the $\sigma^*$ antibonding bulk states. As shown in Fig. 8(c), in the bulk, this state is distributed not only at dimer rows but also between dimer rows and generally does not localize near the dimer atoms, in contrast with the $\pi_1^*$ and $\pi_2^*$ states. In the vacuum region, the corrugation of the EI-LDOS extends slightly above the upper atom. When the sample bias is higher, the position of the spatial distribution forming the STM image is farther from the surface. The LDOS of the $\sigma^*$ states decays more slowly in vacuum than that of the $\pi_1^*$ and $\pi_2^*$ states. Therefore, we predict that the $\sigma^*$ states are evident in the STM images at biases higher than $+2.1$ V.

We have presented the features of the spatial distribution of each state in the LDOS and revealed how the surface and bulk states contribute to STM images. We also demonstrated that the STM image of the clean surface can be interpreted as the isosurface of the spatial distribution of the EI-LDOS in the vacuum region, which is very different from that near the outermost atoms.

## IV. CONCLUSION

We have performed STM observations and theoretical simulations of STM images for the buckled dimer at the $S_A$ step of the clean Si(001) surface. By comparing the experimental results with the theoretical ones, the relationship between STM images and the atomic structure of buckled dimers of the Si(001) surface was clarified. The spatial distributions of the surface and Si-Si bond states in the LDOS were investigated. For the filled states, the $\pi$ ($\pi_1$ and $\pi_2$) surface states contribute to the low-bias STM images and, as the sample bias is increased, the Si-Si bond ($\sigma$) states are added to the $\pi$ states. Since the corrugations of the spatial distributions of the $\pi$ and $\sigma$ states are similar in vacuum, the filled-state images are nearly identical to each other. On the other hand, the empty-state images change considerably with changing sample bias. The STM images obtained at low biases reflect the spatial distribution of the $\pi_1^*$ surface states. As the sample bias is increased, the $\pi_2^*$ surface states begin to dominate the STM images, and a deep trough appears at the center of the dimer at high biases above $+1.3$ eV. Moreover, when the tunneling current is set to be larger, the LDOS nearer to the sample surface contributes to the STM image. These analyses enable us to understand not only STM images but also the electronic structure of the clean Si(001) surface.

## ACKNOWLEDGMENTS

The authors thank H. Goto of Kyoto Institute of Technology for discussing simulation programs. They also thank K. Sugiyama, K. Inagaki, K. Arima, and T. Ishikawa for their great support and useful discussions. This work was supported by a Grant-in-Aid for COE Research (No. 08CE2004) from the Ministry of Education, Science, Sports and Culture.

[1] R. A. Wolkow, Phys. Rev. Lett. **68**, 2636 (1992).
[2] H. Shigekawa, K. Miyake, M. Ishida, K. Hata, H. Oigawa, Y. Nannichi, R. Yoshizaki, A. Kawazu, T. Abe, T. Ozawa, and T. Nagamura, Jpn. J. Appl. Phys., Part 2 **35**, L1081 (1996).
[3] T. Yokoyama and K. Takayanagi, Phys. Rev. B **61**, R5078 (2000).
[4] K. Hata, S. Yasuda, and H. Shigekawa, Phys. Rev. B **60**, 8164 (1999).
[5] R. M. Tromp, R. J. Hamers, and J. E. Demuth, Phys. Rev. Lett. **55**, 1303 (1985); R. J. Hamers, R. M. Tromp, and J. E. Demuth, Phys. Rev. B **34**, 5343 (1986).
[6] H. Tochihara, T. Sato, T. Sueyoshi, T. Amakusa, and M. Iwatsuki, Phys. Rev. B **53**, 7863 (1996).
[7] H. Kageshima and M. Tsukada, Phys. Rev. B **46**, 6928 (1992).
[8] W. Kohn and L. J. Sham, Phys. Rev. **140**, A1133 (1965).
[9] J. P. Perdew and A. Zunger, Phys. Rev. B **23**, 5048 (1981).
[10] N. Troullier and J. L. Martins, Phys. Rev. B **43**, 1993 (1991).
[11] L. Kleinman and D. M. Bylander, Phys. Rev. Lett. **48**, 1425

(1982); K. Hirose and H. Goto (unpublished).
[12] R. Car and M. Parrinello, Phys. Rev. Lett. **55**, 2471 (1985).
[13] J. Tersoff and D. R. Hamann, Phys. Rev. B **31**, 806 (1985).
[14] J. Bardeen, Phys. Rev. Lett. **6**, 57 (1961).
[15] C. J. Chen, in *Introduction to Scanning Tunneling Microscopy*, edited by M. Lapp, J. Nishizawa, B. B. Snavely, H. Stark, A. C. Tam, and T. Wilson, Vol. 4 of *Oxford Series in Optical and Imaging Sciences* (Oxford University Press, New York, 1993).
[16] R. M. Feenstra and J. A. Stroscio, J. Vac. Sci. Technol. B **5**, 923 (1987).
[17] H. Ohnishi, Y. Kondo, and K. Takayanagi, Surf. Sci. **415**, L1061 (1998).
[18] B. Engels, P. Richard, K. Schroeder, S. Blügel, Ph. Ebert, and K. Urban, Phys. Rev. B **58**, 7799 (1998).
[19] S. V. Khare, R. V. Kulkarni, D. Stroud, and J. W. Wilkins, Phys. Rev. B **60**, 4458 (1999).
[20] H. Kim and J. R. Chelikowsky, Phys. Rev. Lett. **77**, 1063 (1996).
[21] J. M. Bass and C. C. Matthai, Phys. Rev. B **52**, 4712 (1995).
[22] W. Lu, P. Krüger, and J. Pollman, Phys. Rev. B **61**, 2680 (2000).
[23] M. Chen, P. G. Clark, Jr., T. Mueller, C. M. Friend, and E. Kaxiras, Phys. Rev. B **60**, 11 783 (1999).
[24] The conventional STM images are measured at tip-sample separations of 5–10 Å (Refs. 16,17). By using the Tersoff-Hamann approximation, the simulated STM images have been generated at separations of 2–4 Å from the outermost atoms, i.e., tip-sample separations that are shorter than the experimental ones (Refs. 18–23). When the behavior of the LDOS of the tip is similar to that of the sample, it is likely that the tunneling current depends more on the sample and the LDOS's of the sample and the tip around the ''middle of the tip-sample distance,'' at which the magnitudes of these LDOS's dominate the tunneling conductance, rather than that at the ''tip'' position. The tip-sample separation is estimated to be about twice as long as that adopted in the Tersoff-Hamann theory and is close to the typical experimental separation.
[25] A. I. Shkrebtii, R. Di Felice, C. M. Bertoni, and R. Del Sole, Phys. Rev. B **51**, 11 201 (1995).
[26] A. Ramstad, G. Brocks, and P. J. Kelly, Phys. Rev. B **51**, 14 504 (1995).
[27] R. Gunnella, E. L. Bullock, L. Patthey, C. R. Natoli, T. Abukawa, S. Kono, and L. S. O. Johansson, Phys. Rev. B **57**, 14 739 (1998).
[28] R. W. Godby, M. Schluter, and L. J. Sham, Phys. Rev. B **37**, 10 159 (1988).
[29] J. E. Northrup, M. S. Hybertsen, and S. G. Louie, Phys. Rev. Lett. **66**, 500 (1991).
[30] L. Kipp, D. K. Biegelsen, J. E. Northrup, L.-E. Swartz, and R. D. Bringans, Phys. Rev. Lett. **76**, 2810 (1996).
[31] L. S. O. Johansson, R. I. G. Uhrberg, P. Mårtensson, and G. V. Hansson, Phys. Rev. B **42**, 1305 (1990).
[32] L. S. O. Johansson and B. Reihl, Surf. Sci. **269/270**, 810 (1992).
[33] T. Yokoyama and K. Takayanagi, Phys. Rev. B **59**, 5212 (1999).
[34] Z. Zhu, N. Shima, and M. Tsukada, Phys. Rev. B **40**, 11 868 (1989).
[35] J. E. Northrup, Phys. Rev. B **47**, 10 032 (1993).
[36] R. J. Hamers, Ph. Avouris, and F. Bozso, Phys. Rev. Lett. **59**, 2071 (1987).
[37] J. J. Boland, Phys. Rev. B **44**, 1383 (1991).
[38] For empty-state images the corrugation minimum appears between dimers, as pointed out by Wolkow, in *Scanning Tunneling Microscopy*, edited by J. A. Stroscio and W. J. Kaiser (Academic Press, San Diego, 1993).
[39] D. J. Chadi, Phys. Rev. Lett. **43**, 43 (1979).